Eur Biophys J
DOI 10.1007/s00249-009-0575-1

ORIGINAL PAPER

Membrane-based actuation for high-speed single molecule force spectroscopy studies using AFM

Krishna Sarangapani · Hamdi Torun · Ofer Finkler · Cheng Zhu · Levent Degertekin

Received: 14 September 2009 / Revised: 1 December 2009 / Accepted: 15 December 2009

Abstract Atomic force microscopy (AFM)-based dynamic force spectroscopy of single molecular interactions involves characterizing unbinding/unfolding force distributions over a range of pulling speeds. Owing to their size and stiffness, AFM cantilevers are adversely affected by hydrodynamic forces, especially at pulling speeds >10 μm/s, when the viscous drag becomes comparable to the unbinding/unfolding forces. To circumvent these adverse effects, we have fabricated polymer-based membranes capable of actuating commercial AFM cantilevers at speeds ≥100 μm/s with minimal viscous drag effects. We have used FLUENT®, a computational fluid dynamics (CFD) software, to simulate high-speed pulling and fast actuation of AFM cantilevers and membranes in different experimental configurations. The simulation results support the experimental findings on a variety of commercial AFM cantilevers and predict significant reduction in drag forces when membrane actuators are used. Unbinding force experiments involving human antibodies using these membranes demonstrate that it is possible to achieve bond loading rates $\geq 10^6$ pN/s, an order of magnitude greater than that reported with commercial AFM cantilevers and systems.

Keywords Hydrodynamic drag · Membrane actuation · Parylene · Cantilever · Unbinding force · Loading rate

Electronic supplementary material The online version of this article (doi:10.1007/s00249-009-0575-1) contains supplementary material, which is available to authorized users.

K. Sarangapani · H. Torun · O. Finkler · L. Degertekin
Woodruff School of Mechanical Engineering,
Georgia Institute of Technology, Atlanta, GA 30332, USA

C. Zhu
Coulter Department of Biomedical Engineering,
Georgia Institute of Technology, Atlanta, GA 30332, USA

Present Address:
K. Sarangapani
Department of Physiology & Biophysics,
University of Washington, Seattle, WA, USA

L. Degertekin (✉)
801, Ferst Drive, Atlanta, GA 30332, USA
e-mail: levent@gatech.edu

Introduction

How proteins function in their microscopic milieu is determined primarily by their structure, but numerous examples of physiological processes exist wherein protein functions are regulated additionally by external factors like mechanical force. A striking example is the force-dependent kinetics of selectin-ligand interactions that mediate the tethering and rolling of leukocytes on vascular endothelia during inflammation or injury (McEver 1991, 2002). Dynamic force spectroscopic studies to characterize unbinding forces or unfolding features of biological macromolecules at the single molecular level using ultrasensitive force probe tools like atomic force microscopy (AFM), biomembrane force probe (BFP) and optical tweezers have been well-documented (Marshall et al. 2003; Sarangapani et al. 2004; Franz et al. 2007; Evans et al. 2004; Chen et al. 2008; Wang et al. 1998). AFM experimental protocols typically involve functionalizing one or both apposing surfaces with molecules of interest, bringing them in contact and pulling them apart to study the forced-dissociation kinetics or domain unfolding patterns. Such studies help to gain insight into the energy landscapes of the interactions tested (Evans and Ritchie 1997; Evans et al. 2001). In order to map the complete energy landscape, the unbinding/unfolding

Published online: 07 January 2010

force distributions over a wide range of loading rates are required.

In AFM experiments, high loading rates can be achieved by using stiffer probes or by increasing the probe retraction speed with a given cantilever, but each approach has its limitation. If one uses commercial small cantilevers, which are usually stiffer, the force resolution has to be compromised, and sophisticated detection systems are required. When using commercial cantilevers especially at pulling speeds >10 μm/s, the hydrodynamic forces acting on the cantilever often compare in magnitude with the unbinding/unfolding forces being measured (Janovjak et al. 2005). Recently, force-clamp spectroscopy measurements have been carried out using the giant muscle protein titin to study the transition state during the protein unfolding process (Dougan et al. 2008). These experiments were conducted in buffer containing glycerol, which is known to enhance protein stability. However, glycerol would make the buffer more viscous and increase drag even at low cantilever pulling speeds. An improved AFM system employing small cantilevers has been reported for imaging and force spectroscopic studies, and retraction speeds as high as 95 μm/s could be reached (Viani et al. 1999a, b). This approach uses specially microfabricated cantilevers with smaller size and lower spring constants (Walters et al. 1996; Viani et al. 1999a, b). Smaller cantilevers are also attractive for various other applications demanding fast operation (Yang et al. 2005; Yamashita et al. 2007; Nakagawa et al. 2009; Katan and Oosterkamp 2008), but these AFM cantilevers and systems are not commercially available yet.

Using different software packages, finite-element method simulations have been performed before with the intention of predicting the dynamic response of cantilevers in liquid (Basak et al. 2006, 2007; Zhang and Turner 2007). In this work, we report drag forces on several commonly used AFM cantilevers computed using FLUENT® (ANSYS® Inc.), the results of which compared well with those from actual experiments. In order to circumvent the hydrodynamic effects often encountered in biological high-speed pulling experiments using commercial AFM cantilevers and systems, we have fabricated membrane-based actuators capable of actuation at very high speeds, with minimal drag effects. Actuating these membranes and using the cantilever as the force sensor allowed us to achieve bond loading rates between human antibodies, an order of magnitude ($\sim 10^6$ pN/s) greater than that reported with commercial AFM cantilevers and systems. Fabrication of parallel arrays of these membranes and the ease of individual actuation would make it possible to conduct experiments with commercial AFM cantilever arrays. This could greatly accelerate the data production rate, minimizing both time and resources input in single molecular research.

Materials and methods

Fabrication of parylene membranes

Polymer membranes used as surface actuators were microfabricated using a Si-based process similar to the fabrication of silicon nitride/oxide membranes previously described (Torun et al. 2007a, b). The membrane structure consists of a stack of parylene (a biocompatible polymer) and aluminium. An embedded aluminium layer on the membrane serves as the top electrode for the integrated electrostatic actuator. The parylene layer completely seals and electrically isolates the actuator when used in fluid and also serves as an ideal surface for anchoring biomolecules, while gold serves as the bottom electrode in the microstructures (Fig. 1a).

Proteins, antibodies and AFM system

Human IgG and anti-human IgG were from Sigma–Aldrich (St. Louis, MO). We used two AFM systems for running experiments, with comparable results. One was built in-house based on a design provided by Vincent Moy (University of Miami, Miami, FL), while the other was a DI 3100 system from Veeco Inc. (Santa Barbara, CA). Both systems employed a laser beam-bounce technique to monitor cantilever deflection (Fig. 1a). AFM cantilevers were from Veeco Inc. (model nos. MLCT and OBL, Olympus Bio-Levers) and calibrated during each experiment using thermal fluctuation analysis (Hutter and Bechhoefer 1993).

Functionalization of AFM cantilevers and membranes in antibody experiments

Membranes were incubated with 10–20 μl of anti-human IgG (10 μg/ml) for 15–20 min at room temperature, and excess antibody was washed off with DPBS (Sigma-Aldrich) containing 1% BSA. AFM cantilevers were incubated with 10 μl of human IgG (10 μg/ml) for 15–20 min at room temperature (Fig. 1b). These concentrations were found to give the right molecular densities to keep binding infrequent and ensure single molecular interactions in the majority of the events tested, in accordance to Poisson statistics (Zhu et al. 2002).

In some experiments, cantilevers were actuated by the piezotranslator (PZT) to bring the tips in contact with the membranes and retract them at different speeds. In other experiments, the membranes were electrostatically actuated to drive them into and out of contact with a stationary cantilever. In either case, binding was signified by the visible bending of the cantilever during the retraction phase, when the tip was linked to the membrane by a molecular bond (*cf.* Fig. 5b). The membrane actuators were reusable: they

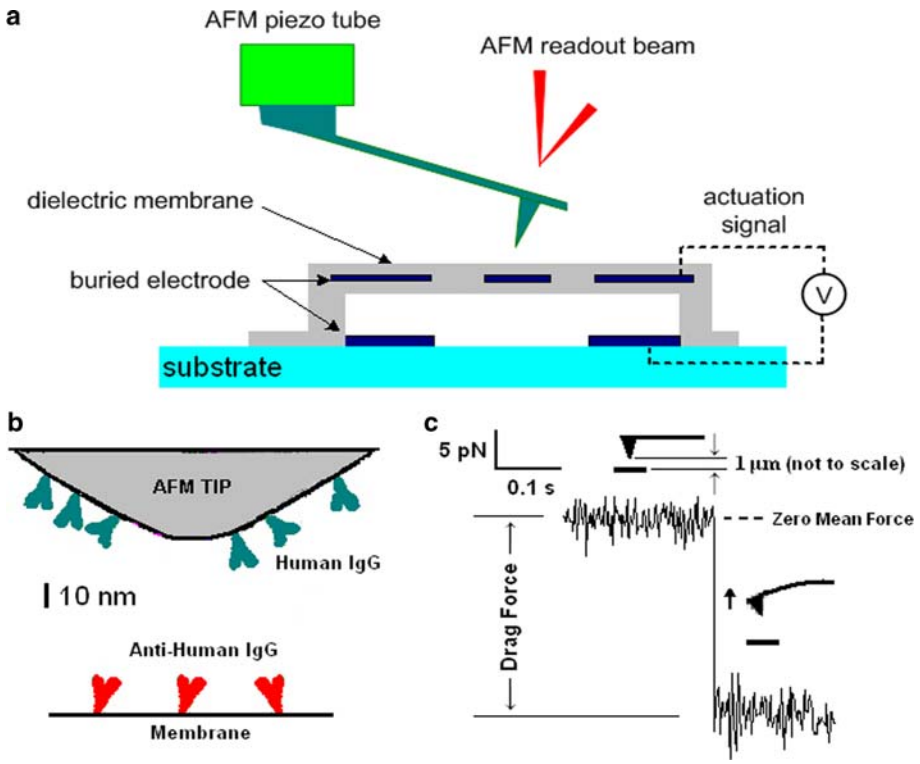

Fig. 1 **a** AFM experimental setup: The experimental unit consists of an (electrostatic) actuation-capable membrane underneath a commercial AFM setup, with the cantilever deflection being monitored continually by conventional laser beam-bounce technique. **b** Functionalization of AFM tip and membrane: In the biomolecular pulling experiments, the cantilever tips were incubated with human IgG, and the membranes were incubated with anti-human IgG (see *Materials and methods*); **c** Drag force measurement: In the force-time scan curve (to be read from left to right), the cantilever is initially held stationary, close to the membrane surface (~1 µm) and subsequently pulled at a set velocity. The deflection of the cantilever (measure of the drag force) is monitored continually. Many such individual pull events were analyzed and data presented as mean ± SEM. The small arrow next to the cantilever indicates the direction of cantilever motion

could be stripped off any biological entities by soaking them in organic solvents after an experiment rendering them ready for a new experiment. All experiments were performed in DPBS buffer containing 1% BSA.

Experimental measurement of drag force

Following contact with the apposing surface (membrane or petri dish), the cantilevers were retracted a set distance (1 µm) from the surface using the PZT and held stationary for some time. Subsequently, they were retracted at different speeds (5, 10, 20 and 40 µm/s), and the cantilever deflection (measure of the drag force) was continually monitored (Fig. 1c). Tens of such individual measurements were recorded at each velocity measure. The experiments were repeated using cantilevers of different shapes and sizes.

Simulations

Details about the FLUENT® simulations have been provided in the supplemental material section (*cf.* Fig. S1).

Results

Drag force on AFM cantilevers during PZT retraction

We used FLUENT® to simulate the hydrodynamic effects on AFM cantilevers during their high speed pulling. Figure S1b–d shows the computational domain for the case of a large triangular cantilever (cantilever C) in proximity (1 µm) to the apposing surface, generated using GAMBIT. Simulations were run for different cantilever shapes and sizes at multiple retraction speeds, and the forces reported by FLUENT® were recorded. To compare with experiments, cantilevers were initially held close (1 µm) to the apposing surface and retracted at the same speed as in the simulations, and the drag forces at each speed were measured (*cf.* Fig. 1c). Drag forces from our home-built AFM (AFM no. 1) and the commercial AFM system (AFM no. 2) had bell-shaped distributions for different cantilever shapes (data not shown) and sizes (Fig. 2a–b). The peak values were close to the mean and moved rightward toward higher forces with increasing cantilever speed regardless of the cantilever shapes (data not shown) and sizes (Fig. 2a–b).

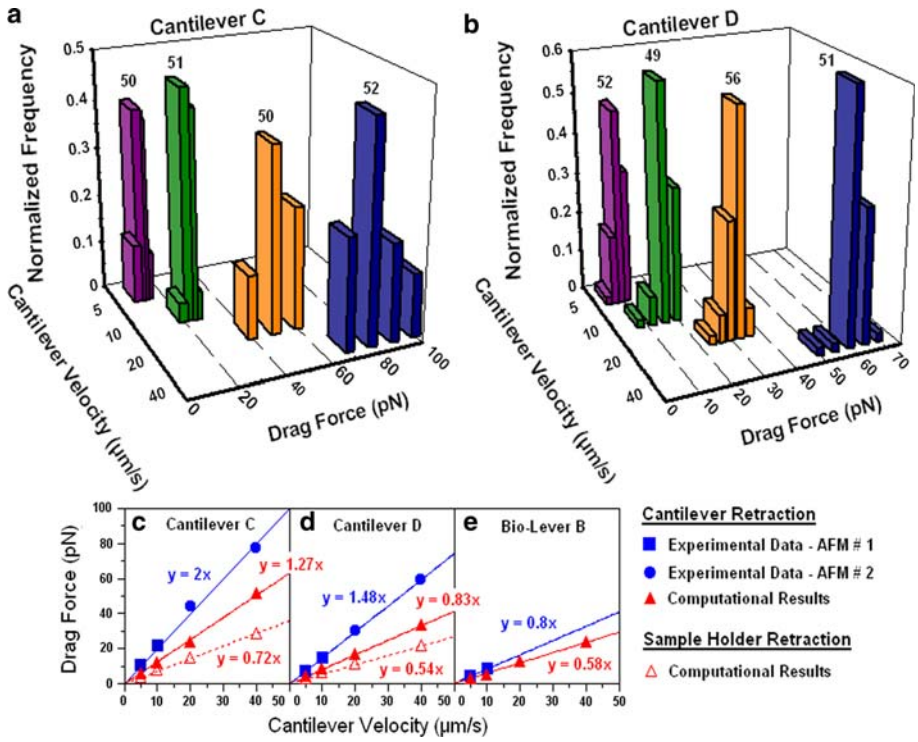

Fig. 2 Drag forces on cantilevers during PZT retraction. (**a**–**b**) Histograms of experimental drag force acting on cantilevers C and D for different cantilever pulling speeds. Each data set has ~50–60 measurements. *Numbers* atop each histogram group represents the number of measurements in that group. The *rightward* shift of the peak upon increasing pulling speed is clearly evident. (**c**–**e**) Drag force vs. cantilever velocity data for triangular and rectangular (Bio-Lever B) cantilevers from experiments (*blue filled squares* and *circles*) and FLUENT® simulations (*red open* and *filled triangles*). Experimental data are presented as Mean ± SEM. In most of the cases, error bars are smaller than the size of symbols. All R^2 values for the linear fits to the data were ≥0.98

Furthermore, reasonable agreements were found between experimentally measured and numerically computed drag forces, both of which increased linearly with cantilever speed for both triangular (Fig. 2c–d) and rectangular (Fig. 2e) cantilevers. The differences between experimental and computed values could be due to several reasons, such as variations in the cantilever thickness within the same batch of cantilevers (please refer to *Supplemental Material* for some results pertaining to this point) or differences in assumptions of buffer viscosity (in the simulations, we specified water as the buffer medium, while in reality, DPBS with 1% BSA could be slightly more viscous than water) as well as changes in buffer viscosity during the course of an experiment due to evaporation of buffer fluid, etc.

Drag force on AFM cantilevers during membrane actuation

To address the adverse hydrodynamic effects on AFM cantilevers at high pulling speeds, we employed actuation-capable membranes in lieu of moving the cantilever. Such polymer-based membranes are capable of actuation speeds >100 μm/s. From Fig. 2c–e, it follows from extrapolation that retracting cantilevers at such speeds would generate many tens to a few hundred pN of drag force on the cantilever, thereby rendering unbinding/unfolding force measurements erroneous if not corrected.

We first performed simulations to determine the drag forces acting on AFM cantilevers when the membranes were actuated in close proximity while keeping the cantilevers stationary. The 3D geometry for the case of a 300-μm diameter membrane at 1 μm distance from triangular cantilever C is shown in Fig. 3a–c (we also performed simulations using cantilever D). Though they look similar, the major difference between Figs. S1b–d and 3a–c is the additional presence of a circular membrane structure underneath the AFM cantilever. Simulations revealed that actuating the membranes would generate much lower drag on the cantilever than if the cantilevers were to be retracted themselves, with the drag forces again scaling linearly with velocity (Fig. 3d, thin dashed and thin solid lines). For example, retracting cantilever C at 50 μm/s would generate a drag force of ~100 pN (*cf.* Fig. 2c), while actuating a 300-μm diameter membrane at the same speed would generate only ~2 pN on cantilever C adjacent to it (Fig. 3d, thin dashed line).

To test these results, we engaged cantilever C with a 300-μm diameter membrane immersed in DPBS buffer. We turned on both the PZT actuator (cantilever) and the electrostatic actuator (membrane), and recorded the displacement of the cantilever from the AFM side. Figure 4a shows the recorded photodiode signal (*y*-axis; converted to force) together with the trajectories of the cantilever and the membrane during one such run. The PZT covered a peak-to-peak displacement of 1.3 μm at ~20 μm/s, while the membrane was actuated at a similar speed with a 70-nm peak-to-peak displacement. The recorded force curve clearly shows that the cantilever and membrane made the

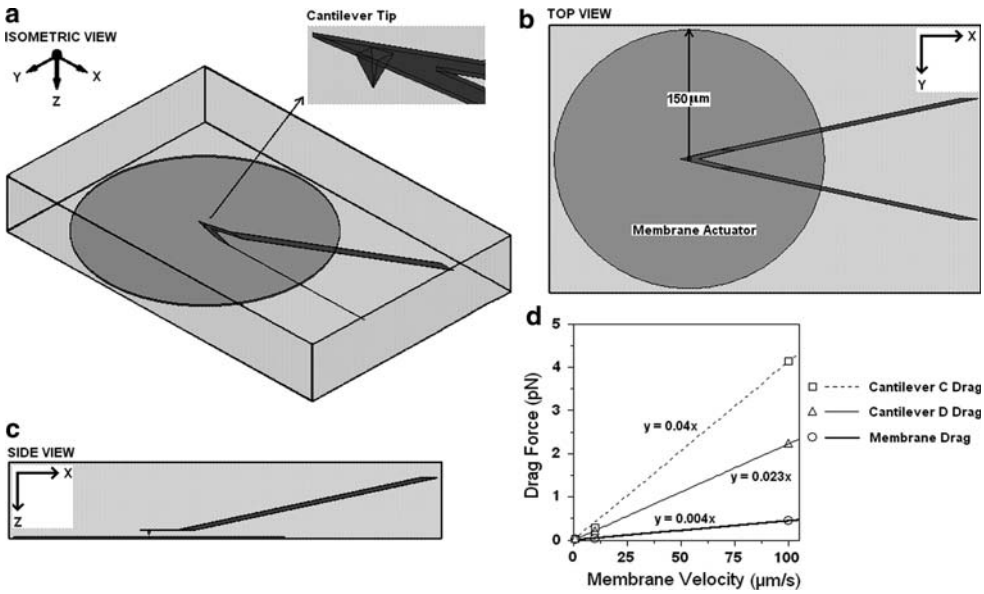

Fig. 3 **a–c** Two- and three-dimensional views of the computational domain geometry. Cantilever C and a 300-µm diameter membrane have been used for illustration. The cantilever beam length, width and thickness as well as tip dimensions used in the simulations are in accordance with manufacturer-reported values. **d** Computed drag forces on AFM cantilevers C and D and membranes due to membrane actuation. Note that the drag force on cantilevers is ~50–60-fold lower than in the cases in Fig. 2c–d

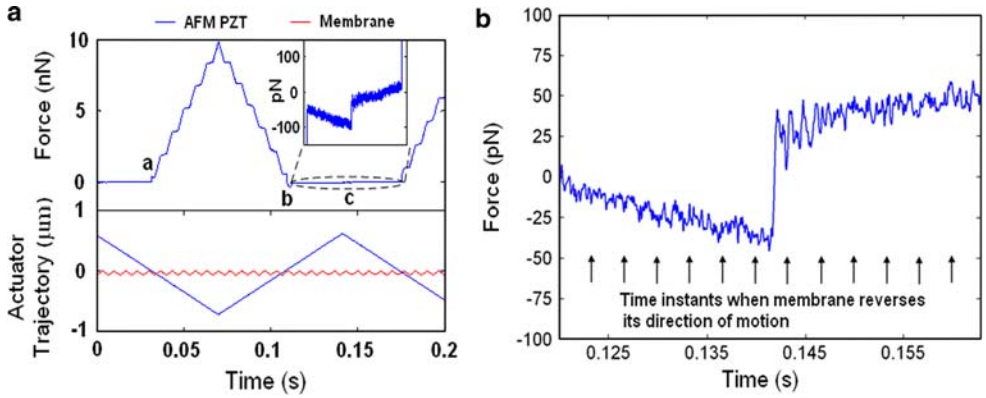

Fig. 4 **a** Force (*top*) and displacement (*bottom*) trajectories of PZT and membrane actuators. A visible hydrodynamic drag (as signified by a kink in the force-time trace; see *inset*) manifests during PZT actuation, while membrane actuation at comparable speed does not impact the adjacent cantilever in any discernible manner. **b** Amplified portion of trace from inset in panel (**a**) (see text for details). The time instants when the membrane reverses its direction are labeled by small *arrows* for clarity

first contact at ~0.03 s (point a), and the resultant displacement of the cantilever (from point a to point b) is due to the superposition of both PZT and membrane actuators when the structures were in contact. Point b refers to the instant when the cantilever and membrane get out of contact. At point c (~0.14 s), the PZT reverses its direction. The inset corresponding to time duration marked with dashed lines shows an amplified portion of the force curve clearly featuring the effect of cantilever drag that manifests as a visible jump in the force curve when the PZT reverses direction. However, whenever the membrane moving at a similar speed reverses its direction, the resultant drag force on the cantilever is not resolvable (<5.84 pN rms noise level, based on our calculations), which clearly corroborated our computational results. The portion of the trace in the inset has been filtered and amplified further in Fig. 4b to further illustrate this point. The force trace shows no measurable hydrodynamic drag force when the membrane actuator reverses its direction.

In the simulations pertaining to Fig. 3, the tip of the cantilever was exactly positioned over the center of the underlying membrane, but achieving this experimentally is challenging. To assist us with cantilever positioning, the membrane actuators were fabricated with a small metal area under the dielectric layer located at the center. During the experiments, we could clearly see this metal layer and engage the cantilever accordingly, giving us confidence about the measurements.

According to the small deflection theory of thin plates, the deflection of the membranes can be expressed by a Bessel function with a maximum deflection at the center and zero at the periphery (Leissa 1993). The membrane actuators used in the present work were moved ~100 nm at the center though these actuators have a much higher range

(∼1 μm). Moving localized areas of the membrane by such small distances would push only a very small volume of liquid out in its immediate milieu and create a small flow field. On the contrary, when an AFM cantilever moves with its base, it would create more complicated flow-like conditions, generating a strong resistance to its motion that would manifest as a large drag. This theory is supported by velocity profile and pressure contour analyses of cantilever and membrane during their respective actuation (see *Supplemental Material*; Figs. S2 and S3). Taken together, the results from Figs. 2, 3 and 4 suggested that membrane actuation would serve as a much better alternative to cantilever retraction, especially in biological fast pulling experiments.

Binding specificity in antibody pulling experiments

To confirm specificity of the interactions, BSA-coated cantilevers, when tested against anti-human IgG-incubated membranes, showed ∼5% adhesion (Fig. 5a). Coating the cantilevers with human IgG greatly increased the adhesion probability to ∼35%, while blocking the membranes with excess human IgG in solution resulted in a dramatic drop of adhesion probability between the same membrane-tip pair at par with nonspecific levels (Fig. 5a). The majority of the adhesions between human IgG-coated cantilevers and anti-human IgG-incubated membranes exhibited a single peak or rupture, with a progressively smaller number of events with multiple peaks, in accordance with Poisson statistics (data not shown). This suggested that majority of the adhesion events tested involved single molecular interactions (Zhu et al. 2002).

Unbinding force studies by membrane actuation

The exponential augmentation of bond dissociation due to applied force results in an increase in bond strength with loading rate (Evans and Ritchie 1997; Evans et al. 2001; Zhang et al. 2004, Wojcikiewicz et al. 2006). To map the energy landscape of the molecular interaction in question via dynamic force spectroscopy, it is imperative that the rupture forces are measured over a very wide range of bond loading rates. Initially, we recorded force spectroscopy data for human IgG interactions with a counter antibody (anti-human IgG) employing cantilevers (C and D) over a range of retraction speeds till hydrodynamic effects set in. The cantilevers were used both for actuation and force sensing. In trying to reach 10^5 pN/s loading rate, we had to retract the cantilevers at speeds >10 μm/s, encountering few tens of pN drag force in the process.

To sidestep the hydrodynamics issue, we actuated the membranes at speeds between 10 and 100 μm/s by applying voltages <50 V while the stationary cantilever was used only for force sensing. Figure 5b shows a force-time trace of the signal from the AFM cantilever when a 300-μm diameter membrane was actuated at a speed of ∼100 μm/s in its proximity. The minimal hydrodynamic drag on the AFM cantilever is strongly demonstrated by the cantilever snapping back to its mean resting position (horizontal black line) immediately after bond rupture, while the membrane was moving at ∼100 μm/s. Loading rate was obtained directly from the slope of the linear portion of the force-time scan curve (Fig. 5b).

Many such unbinding force measurements involving both cantilever and membrane actuation were pooled from multiple experiments involving different tip-membrane pairs to ensure statistical robustness. Histograms of the unbinding forces had a characteristic bell distribution, with the peak shifting rightward toward increasing forces with increasing loading rate (Fig. 5c). With membrane actuation, we measured bond-loading rates from 10^4 pN/s to as high as 10^6 pN/s, an order of magnitude higher than that possible with cantilever pulling (Fig. 5c–d). Data from membrane actuation experiments compared well with those from cantilever pulling experiments (see overlapping data points from AFM and membrane actuation at ∼10^4 pN/s in Fig. 5d). Furthermore, a plot of the peak value of the unbinding force distributions vs. loading rate was linear (semi-log axes plot) with a solitary segment (Fig. 5d), suggesting that these interactions had a single energy barrier under the conditions tested (Evans and Ritchie 1997; Evans et al. 2001; Zhang et al. 2004; Wojcikiewicz et al. 2006). Furthermore, the unbinding forces measured in our experiments are in the range of rupture forces reported for other antigen-antibody pairs (Dammer et al. 1996; Idiris et al. 2005; Marshall et al. 2005). We believe that our membrane-based experimental protocol can be applied to characterize the dynamic force spectroscopic properties of other molecular systems as well.

Discussion

We have systematically characterized the hydrodynamic effects because of respective cantilever and membrane actuations based on simulations and experiments. In our simulations, we positioned the cantilever 1 μm from the adjacent surface. This is because while modeling the cantilever in GAMBIT, we faced a problem to mesh the geometry when the cantilever was brought very close to the surface (<1 μm). Though analytical models predict infinite drag forces when the separation of a moving structure and an adjacent solid boundary vanishes, Janovjak et al. (Janovjak et al. 2005) have shown that the drag force increases ∼1.5-fold when the cantilever tip-surface separation decreases from 2.5 μm to 0. Based on these results we do not expect a significant (i.e., orders of magnitude)

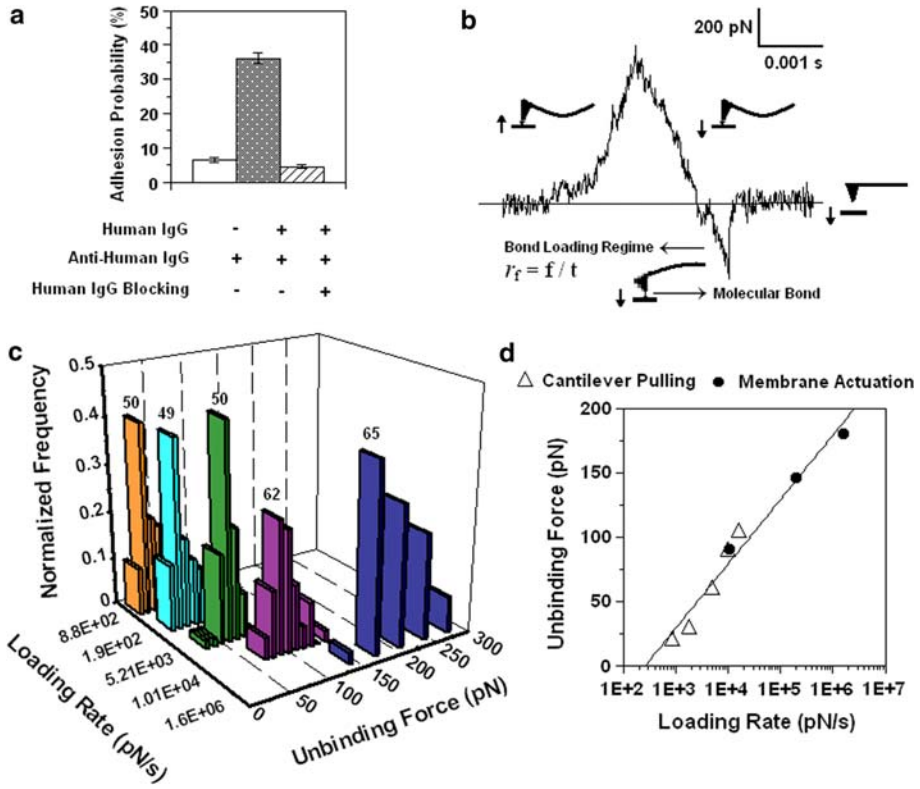

Fig. 5 **a** Binding specificity in antibody experiments. Initially, the membranes were coated with anti-human IgG and tested against non-functionalized AFM cantilever tips (*white open bar*: absence of function). In the next step, the cantilevers were functionalized with human IgG (*patterned bar*: gain of function). Finally, the cantilever tips were incubated with excess anti-human IgG and tested again (*hatched bar*: loss of function). **b** A typical force-time trace obtained with membrane actuation (to be read from *left to right*). In the left ascending portion of the trace, the membrane moves upward (depicted by the small *arrow* next to it), causing the cantilever to bend upward (compression). In the subsequent descending portion, the membrane reverses its direction of motion, but the cantilever is still bent upward. Further downward motion of the membrane beyond the zero mean force position (*horizontal black line*) causes the cantilever to bend downward (tension) due to a biomolecular bond linkage. Upon bond rupture, the cantilever snaps back to its resting position immediately without any visible hydrodynamic effects though the membrane is moving at a very high speed. **c** Unbinding force histograms for human IgG vs. anti-human IgG interactions at multiple bond loading rates. The *rightward* shift of the peak position with increasing bond loading rate is clearly evident. The data set for the highest loading rate (*blue bars*) were obtained with membrane actuation, while all other data sets were obtained with cantilever retraction. The cantilever was used as the force sensor in all the cases. *Numbers* atop each histogram group represent the number of measurements in that group. **d** Strength spectrum of human IgG vs. anti-human IgG interactions reveals a linear trend for bond loading rates spanning ~4 orders of magnitude. R^2 value for the linear fit to the data was 0.96

increase in the drag force when the cantilever is close to the adjacent surface. Also, in our simulations, we had the cantilever untethered to the adjacent surface. This is also justified since the origin of the drag force in the simulations is not due to the actual bending of the cantilever (wall zones are infinitely rigid in the computations), but rather a reaction to the flow because of its rigid translational motion including the base.

Though hydrodynamic forces increased with actuation speed, membranes were much less impacted by hydrodynamic effects compared to cantilevers with comparable dimensions. Moving only the top face of the membrane that is exposed to the fluid would push only a very small volume of liquid out in its immediate milieu and create a small flow field. On the contrary, when an AFM cantilever moves with its base, it could create more complicated flow-like conditions, generating a strong resistance to its motion that would manifest as a large drag. This theory is supported by velocity profiles and pressure contours on the AFM cantilever or membrane actuator (obtained from FLUENT®). These results have been presented in the *Supplemental Material* section (*cf.* Figs. S2 and S3).

Fabricating the membrane actuators entails a detailed protocol, and each membrane requires calibration before use. Also, the addition of an actuator device adds to the complexity of the experimental setup. However, one can still use our membrane actuators with commercial AFM cantilevers and systems while monitoring cantilever deflection using the traditional AFM optical readout method, as in this work. Another possible drawback with our membrane-based actuator system is the energy that can be coupled to the surrounding fluid from vibrating the membrane at high

frequencies, which could potentially impact the kinetics of the molecular system being studied. However, we note that this would be of concern at frequencies wherein the membrane size is comparable to acoustic wavelength (e.g., >1 MHz for a 300-μm diameter membrane). The experiments reported here were conducted at 1 kHz, and this effect is not of significant concern here.

It is also possible to monitor the membrane actuator displacement with high resolution using an integrated grating based interferometer as described earlier (Torun et al. 2007a, b). With this capability, the membrane actuator can provide information about molecular extensions and may be used both as an actuator and force sensor.

Conclusions

We have fabricated membrane-based actuation structures for high-speed pulling dynamic force spectroscopic experiments that exhibit significantly reduced hydrodynamic interference as compared to common AFM cantilevers that are moved by piezoelectric actuators. We have developed a detailed model to calculate the hydrodynamic drag on several commonly used AFM cantilevers in different force spectroscopy experiment configurations and compared the results with experimental data. The comparisons showed that the model captured essential features of the drag force, and hence it could be extended to simulate hydrodynamic drag in systems where a membrane actuator is used. The results on membrane actuator driven experiments indeed showed an order of magnitude lower drag forces, enabling loading biomolecular bonds at rates $\geq 10^6$ pN/s. Membrane actuator-driven antibody pulling experiments further showed the applicability of the approach for conducting force spectroscopy on a variety of biomolecules. The low drag forces on the membrane, coupled with a sensitive displacement sensing scheme that has been demonstrated earlier, suggest that these membrane-based systems can be used as force sensors as well actuators for improved force spectroscopy involving single biomolecules.

Acknowledgments We thank Dr. Fang Kong and Jiangguo Lin for help with data collection. We also thank Dr. Peter Kottke for helpful discussions involving FLUENT®. This work was supported by the National Institutes of Health (AI060799).

References

Basak S, Raman A, Garimella SV (2006) Hydrodynamic loading of microcantilevers vibrating in viscous fluids. J Appl Phys 99: 114906 (1–10). doi: 10.1063/1.2202232

Basak S, Beyder A, Spagnoli C, Raman A, Sachs F (2007) Hydrodynamics of torsional probes for atomic microscopy in liquids. J Appl Phys 102:024914 (1–7). doi: 10.1063/1.2759197

Chen W, Evans E, McEver RP, Zhu C (2008) Monitoring receptor-ligand interactions between surfaces by thermal fluctuations. Biophys J 94:694–701. doi:10.1529/biophysj.107.117895

Dammer U, Hegner M, Anselmetti D, Wagner P, Dreier M, Huber W, Güntherodt HJ (1996) Specific antigen/antibody interactions measured by force microscopy. Biophys J 70:2437–2441. doi:10.1016/S0006-3495(96)79814-4

Dougan L, Feng G, Hui Lu, Fernandez JM (2008) Solvent molecules bridge the mechanical unfolding transition state of a protein. Proc Natl Acad Sci USA 105:3185–3190. doi:10.1073/pnas.0706075105

Evans E, Ritchie K (1997) Dynamic strength of molecular adhesion bonds. Biophys J 72:1541–1555. doi:10.1016/S0006-3495(97)78802-7

Evans E, Leung A, Hammer D, Simon S (2001) Chemically distinct transition states govern rapid dissociation of single L-selectin bonds under force. Proc Natl Acad Sci USA 98:3784–3789. doi:10.1073/pnas.061324998

Evans E, Leung A, Heinrich V, Zhu C (2004) Mechanical switching and coupling between two dissociation pathways in a P-selectin adhesion bond. Proc Natl Acad Sci USA 101:11281–11286. doi:10.1073/pnas.0401870101

Franz CM, Taubenberger A, Puech PH, Müller DJ (2007) Studying integrin-mediated cell adhesion at the single-molecule level using AFM force spectroscopy. Sci STKE 406:p15. doi:10.1126/stke.4062007pl5

Hutter JL, Bechhoefer J (1993) Calibration of atomic-force microscope tips. Rev Sci Instrum 64:1868–1873. doi:10.1063/1.1144449

Idiris A, Kidoaki S, Usui K, Maki T, Suzuki H, Ito M, Aoki M, Hayashizaki Y, Matsuda T (2005) Force measurement for antigen-antibody interaction by atomic force microscopy using a photograft-polymer spacer. Biomacromolecules 6:2776–2784. doi:10.1021/bm0502617

Janovjak H, Struckmeier J, Müller DJ (2005) Hydrodynamic effects in fast AFM single-molecule force measurements. Eur Biophys J 34:91–96. doi:10.1007/s00249-004-0430-3

Katan AJ, Oosterkamp TH (2008) Measuring hydrophobic interactions with three-dimensional nanometer resolution. J Phys Chem C 112:9769–9776. doi:10.1021/jp711017n

Leissa AW (1993) Vibration of plates (NASA SP-160). Government printing office, Washington, US. Reprinted by The Acoustical Society of America

Marshall BT, Long M, Piper JW, Yago T, McEver RP, Zhu C (2003) Direct observation of catch bonds involving cell-adhesion molecules. Nature 423:190–193. doi:10.1038/nature01605

Marshall BT, Sarangapani KK, Lou J, McEver RP, Zhu C (2005) Force history dependence of receptor-ligand dissociation. Biophys J 88:1458–1466. doi:10.1529/biophysj.104.050567

McEver RP (1991) Selectins: novel receptors that mediate leukocyte adhesion during inflammation. Thromb Haemost 65:223–228

McEver RP (2002) Selectins: Lectins that initiate cell adhesion under flow. Curr Opin Cell Biol 14:581–586

Nakagawa K, Hashiguchi G, Kawakatsu H (2009) Small single-crystal silicon cantilevers formed by crystal facets for atomic force microscopy. Rev Sci Instrum 80:095104–095105. doi:10.1063/1.3202322

Sarangapani KK, Yago T, Klopocki AG, Lawrence MB, Fieger CB, Rosen SD, McEver RP, Zhu C (2004) Low force decelerates L-selectin dissociation from P-selectin glycoprotein ligand-1 and endoglycan. J Biol Chem 279:2291–2298. doi:10.1074/jbc.M310396200

Torun H, Sutanto J, Sarangapani KK, Joseph P, Degertekin FL, Zhu C (2007) Micromachined membrane-based active probe for biomolecular mechanics measurement. Nanotechnology 18:165303 (1–8). doi: 10.1088/0957-4484/18/16/165303

Torun H, Sarangapani KK, Degertekin FL (2007) Spring constant tuning of active atomic force microscope probes using electrostatic

spring softening effect. Appl Phys Lett 91:253113 (1–3). doi:10.1063/1.2827190

Viani MB, Schäffer TE, Paloczi GT, Pietrasanta LI, Smith BL, Thompson JB, Richter M, Rief M, Gaub HE, Plaxco KW, Cleland AN, Hansma HG, Hansma PK (1999a) Fast imaging and fast force spectroscopy of single biopolymers with a new atomic force microscope designed for small cantilevers. Rev Sci Instrum 70:4300–4303. doi:10.1063/1.1150069

Viani MB, Schäffer TE, Chand A, Rief M, Gaub HE, Hansma PK (1999b) Small cantilevers for force spectroscopy of single molecules. J Appl Phys 86:2258–2262. doi:10.1063/1.371039

Walters DA, Cleveland JP, Thomson NH, Hansma PK, Wendman MA, Gurley G, Elings V (1996) Short cantilevers for atomic force microscopy. Rev Sci Instrum 67:3583–3590. doi:10.1063/1.1147177

Wang MD, Schnitzer MJ, Yin H, Landick R, Gelles J, Block SM (1998) Force and velocity measured for single molecules of RNA polymerase. Science 282:902–907. doi:10.1126/science.282.5390.902

Wojcikiewicz EP, Abdulreda MH, Zhang X, Moy VT (2006) Force spectroscopy of LFA-1 and its ligands, ICAM-1 and ICAM-2. Biomacromolecules 7:3188–3195. doi:10.1021/bm060559c

Yamashita H, Kodera N, Miyagi A, Uchihashi T, Yamamoto D, Ando T (2007) Tip-sample distance control using photothermal actuation of a small cantilever for high-speed atomic force microscopy. Rev Sci Instrum 78:083702–083705. doi:10.1063/1.2766825

Yang JL, Despont M, Drechsler U, Hoogenboom BW, Frederix PLTM, Martin S, Engel A, Vettiger P, Hug HJ (2005) Miniaturized single-crystal silicon cantilevers for scanning force microscopy. Appl Phys Lett 86:134101–134103. doi:10.1063/1.1895482

Zhang W, Turner K (2007) Frequency dependent fluid damping of micro/nano flexural resonators: Experiment, model and analysis. Sens Actuators A: Phys 134:594–599. doi:10.1016/j.sna.2006.06.010

Zhang X, Craig SE, Kirby H, Humphries MJ, Moy VT (2004) Molecular basis for the dynamic strength of the integrin $\alpha 4\beta 1$/VCAM-1 interaction. Biophys J 87:3470–3478. doi:10.1529/biophysj.104.045690

Zhu C, Long M, Chesla SE, Bongrand P (2002) Measuring receptor/ligand interaction at the single-bond level: Experimental and interpretative issues. Ann Biomed Eng 30:305–314. doi:10.1114/1.1467923